Citation: Herreid, Samuel and Pellicciotti, Francesca (2020) The state of rock debris covering Earth’s glaciers. Nature Geoscience, 13 (9). pp. 621-627. ISSN 1752-0894

Published by: Nature Publishing

URL: https://doi.org/10.1038/s41561-020-0615-0 <https://doi.org/10.1038/s41561-020-0615-0>

Manuscript #: NGS-2019-11-02761A

Corresponding author name(s): Sam Herreid

1. Extended Data

Figure #	Figure title One sentence only	Filename This should be the name the file is saved as when it is uploaded to our system. Please include the file extension. i.e.: *Smith_ED_Fi_1.jpg*	Figure Legend If you are citing a reference for the first time in these legends, please include all new references in the Online Methods References section, and carry on the numbering from the main References section of the paper.
Extended Data Fig. 1	Extended Data Fig 1. Landsat satellite imagery used to map debris cover.	Herreid_ED_01_Fig1.jpg	The footprint of each manually selected Landsat image is shown colored by the date of acquisition. The histogram inset shows the number of scenes per year differentiated by sensor and is broken down per region in the Supplemental Information.
Extended Data Fig. 2	Extended Data Fig 2. Landsat image coverage with no overlap.	Herreid_ED_02_Fig2.jpg	Landsat image footprints over Alaska and Western Canada are outlined and colored by acquisition data illustrating the preference given to more recent imagery and the removal of overlapping image area.
Extended Data Fig. 3	Extended Data Fig 3. Amending the RGI v6.0.	Herreid_ED_03_Fig3.jpg	Southern Andes as an example of the manual steps taken to identify and remove FP glacier error, area in shadow and cloud covered area; and identify and add FN errors in every RGI region. The wider shapes, or lassos, were used to tag enclave shapes initially mapped as 'debris cover' with a specific error

			or true (by omission) classification. This lasso approach enables the manual work conducted in this study to be used again in future inventories with any desired modifications.
Extended Data Fig. 4	Global debris cover results and errors in RGI v6.0 presented as regional percentages.	Herreid_ED_04_Table 1.jpg	All values are given for glaciers with a surface area greater than or equal to 1 km^2 that fall within the considered spatial domain. '% RGI6.0 considered' is unedited RGI v6.0 glacier area with i. glaciers smaller than 1 km^2 removed and ii. area outside of the Landsat image composite (Extended Data Fig. 1) removed divided by entirely unaltered RGI v6.0 glacier area. '% SamRGI considered' is the edited glacier area within the Landsat image composite divided by the edited glacier area inside and outside of the Landsat image composite.
Extended Data Fig. 5	Global debris cover results and errors in the RGI v6.0 presented as areas (km^2).	Herreid_ED_05_Table 2.jpg	Glacier area includes corrections to the RGI. These results exclude glaciers with a surface area less than 1 km^2. Glacier area in shadow, including other visually uncertain shapes classified as debris, were removed from the debris map but not removed from the RGI.
Extended Data Fig. 6	Extended Data Fig 4. Estimation of the equilibrium line from mapped debris cover.	Herreid_ED_06_Fig4.jpg	Map view and cross-section cartoon illustrating the method used in this study to estimate the position of the equilibrium line for glaciers with 7% debris cover and/or >10 km^2 debris-covered area. Equilibrium line is estimated by locating the upper-most debris exposure, extending the point of exposure to the full glacier width and adjusting the position up-glacier by a factor of *d*. *d* is the glacier specific distance between the true equilibrium line and the first down-glacier emergence of englacial debris.
Extended Data Fig. 7	Extended Data Fig 5. Cases where the	Herreid_ED_07_Fig5.j	Landsat image of glaciers in Svalbard (a) and corresponding results from this study (b) showing examples of where

	equilibrium line location estimates are incorrect.	pg	equilibrium line estimates (yellow line) derived from mapped debris cover fails. Equilibrium lines shown on grey glaciers did not meet the 7% debris cover and/or >10 km^2 debris-covered area criteria and were not included in any further metric derivation or results. Glaciers shown as blue met the criteria to be included in the study but also are shown to have errors. The source for error include (1) sparse debris cover producing nonsensical equilibrium lines; (2) imperfect flow divides drawn in ambiguous cases within RGI v6.0 causing unphysical equilibrium line estimates; (3) the unusual case where debris cover is present up-glacier but is not sufficiently present at lower reaches of the glacier to be detected by the debris mapping algorithm; (4) a portion of a glacier's ablation zone is debris free and big enough to cause the glacier width buffer to inaccurately extend the ablation zone area to encompass the full width of the glacier. While this sample region was selected due to a concentration of errors, (5) shows a location where equilibrium line location was predicted as intended.
Extended Data Fig. 8	Extended Data Fig 6. Comparison between the global debris map presented here and the global debris map from (ref. [18]).	Herreid_ED_08_Fig6.jpg	Error, true positive rate and precision are calculated under the assumption that results from this study are correct. The basis of this assumption is the additional manual editing that was conducted within this study, where (ref. [18]) used unaltered RGI v6.0. Greenland was excluded from the comparison due to the different spatial domains considered. The values used to make this figure are given in the Supplemental Information.
Extended Data Fig. 9	Extended Data Fig 7. Examples illustrating errors in the RGI and (ref. [18]).	Herreid_ED_09_Fig7.jpg	Two example locations are shown to illustrate a setting where heavy editing to the RGI was required (Central Asia) and almost no editing of the RGI was required (Alaska). The bottom two panels show the comparison of results from this study and those of (ref. [18]). A clear undercounting of debris by (ref. [18]) is apparent in both regions where in Alaska the methods of (ref. [18]) are examined without influence from the

			RGI editing conducted in this study while the errors in Central Asia show a compound error in (ref. [18]) composed of both an undercounting of true debris cover and an over counting where off-glacier area is erroneously classified as debris cover.

2. Supplementary Information:

A. Flat Files

Item	Present?	Filename This should be the name the file is saved as when it is uploaded to our system, and should include the file extension. The extension must be .pdf	A brief, numerical description of file contents. i.e.: *Supplementary Figures 1-4, Supplementary Discussion, and Supplementary Tables 1-4.*
Supplementary Information	Choose an item.	Herreid_R2_SI.pdf	Supplementary Text Figures S1 to S6 Tables S1 to S4 Description of Data S1 to S3 Supplementary References
Reporting Summary	Choose an item.		

The state of rock debris covering Earth's glaciers

Sam Herreid[1,2*], Francesca Pellicciotti[2,1]

[1]Department of Geography, Faculty of Engineering and Environment, Northumbria University, Newcastle upon Tyne, UK.

[2]Swiss Federal Research Institute WSL, Birmensdorf, Switzerland

*Correspondence to: samherreid@gmail.com

Rock debris can accumulate on glacier surfaces and dramatically reduce glacier melt. The structure of a debris cover is unique to each glacier and sensitive to climate. Despite this, debris cover has been omitted from global glacier models and forecasts of their response to a changing climate. Fundamental to resolving these omissions is a global map of debris cover and an estimate of its future spatial evolution. Here we use Landsat imagery and a detailed correction to the Randolph Glacier Inventory to show that 7.3% of mountain glacier area is debris-covered and over half of Earth's debris is concentrated in three regions: Alaska (38.6% of total debris-covered area), Southwest Asia (12.6%) and Greenland (12.0%). We use a set of new metrics including *stage*, the current position of a glacier on its trajectory towards reaching its spatial debris cover carrying capacity, to quantify the state of glaciers. Debris cover is present on 44% of Earth's glaciers and prominent (>1.0 km^2) on 15%. 20% of Earth's glaciers have a substantial percentage of debris cover for which net *stage* is 36% and the bulk of individual glaciers have evolved beyond an optimal moraine configuration favorable for debris cover expansion. Use of this dataset in global scale models will enable improved estimates of melt over 10.6% of the global glacier domain.

A layer of rock debris on the surface of a glacier causes a diminishing sub-debris melt rate as the layer thickness varies from ~2 cm to meters thick[1-3]. This relation has been established since 1959, yet a consideration of supraglacial rock debris has been a long-standing omission from global scale glacier models[4] often citing its heterogeneous properties and assumed sparse global distribution as justification. Beyond the problem of resolving basic debris geometry, as a debris cover increases in extent it can support the development of ice cliffs and supraglacial ponds which have been shown to accelerate the local melt rate[5,6] and add complexity to the advanced stages of debris cover evolution[7]. While an omission of debris cover was necessary to arrive at the first operative global scale models, a consideration of debris cover, summed over Earth's glaciers, has the potential to reveal that earlier estimates of glacier-sourced eustatic sea level rise were too high. Additionally, hydrological models will likely underestimate the longevity of glacier sourced water resources if debris cover, and its evolution, is neglected.

While the structure of the debris present on any one glacier is a unique and complex function of many local factors including the surrounding geology, topographic relief and glacier dynamics[8], a consensus of studies from around the world show a spatial expansion of debris cover and link this change to a warming climate[9-16]. Between the evidence that debris cover is expanding and its omission in global glacier models, there are three remaining fundamental unknowns that need to be resolved in order to close this knowledge gap: the spatial distribution, thickness and 3-D evolution of supraglacial debris. Very few prior studies have quantified debris cover at a global scale[17,18]. These studies relied on fully automated, big data techniques that either lack agreement to repeat measurements (Extended Data Fig. 6, 7, Supplementary Material) or were not published. A global scale consideration of the trajectory debris cover may follow as it evolves in the future has never been addressed. Here, we take the opposite of a big data approach and apply a semi-automated method to carefully selected satellite images with iterative and manually intensive steps to mitigate several sources of error that are difficult to automate including inaccurate/outdated glacier outlines, cloud cover and topographic shading. We use these results to address two of the global unknowns: the spatial distribution and 2-D evolution trajectory of debris cover.

Global distribution of debris cover

Multispectral satellite imagery and a map of glacier area can be used as input to a simple image segmentation approach to map debris cover[19,20]. The strong color contrast between rocks and glacier ice, firn and snow enables a robust and repeatable method to map debris cover, provided the glacier map is accurate and the imagery is controlled for factors including seasonal snow and cloud cover (Methods Section 1.1). With the 2014 release of the global Randolph Glacier Inventory[21] (RGI), hereafter referring to version 6.0 (ref. [22]), it became feasible to map debris cover globally using this method[18]. However, a preliminary qualitative investigation for this study suggested that the RGI inconsistently constrained the glacier area visible in a manually selected, overlap-free global coverage of Landsat imagery (n = 255, acquired between 1986-2016, median = 2013, Methods Sections 1.1-1.3, Extended Data Fig. 1, 2 Supplemental Information), and thus was of insufficient quality to map debris cover (Extended Data Fig. 7). To address and quantify this deficiency, we updated the RGI (with a conditional inclusion of the entire Greenland ice sheet, exclusion of Antarctica and exclusion of all glaciers with a surface area <1 km^2, Methods Section 1.4, 1.10) by generating a first iteration global debris cover map which defined the shape of all non-bare-ice area within the RGI. We then, in a time intensive step, manually differentiated these shapes between true positive debris cover, land that is not glacier (RGI false positive) and topographically shaded area (Methods Sections 1.4-1.10, Extended Data Fig. 3, 8). Glacier area missing from the RGI (false negative glacier area) was digitized manually. False positive and false negative errors within the RGI summed to 11,483 km^2 or 3.3% of glacier area (Extended Data Tables 1, 2) and their removal along with shaded and clouded area enabled the derivation of a final, refined and temporally consistent glacier and debris cover map showing 7.3% of Earth's mountain glacier area is covered by rock debris (Fig. 1, Methods Section 1.11, Extended Data Tables 1, 2). This result is distinctly higher than the only previously published global debris cover map[18]. A comparison analysis with [18] shows a systematic undercounting of debris cover where 51% of the debris cover mapped in this study was missed by [18] and 25% of the debris mapped by [18] was not classified as debris in this study (Extended Data Fig. 6, 7, Supplemental Information). A comparison analysis with the regional debris cover map from [23], who included debris cover in a full glacier model for all High Mountain Asia, shows a higher, 81% coincidence with the debris cover mapped in this study and a false discovery rate of 29% (Supplemental Data). Both comparison analyses with [18] and [23] overcount error where these studies correctly identified debris cover that is missed in this study.

Of the glaciers on Earth with a surface area >2 km^2, 44% have some debris cover (>0.1 km^2) and 15% have a prominent debris cover (>1.0 km^2; Fig. 1a). 20% of Earth's glaciers with a surface area >2 km^2 have a 'substantial' debris cover (>7% debris-covered and/or >10 km^2 of debris) which we define to make debris cover dependent calculations. Considering only this 20% of Earth's glaciers, the percentage of debris-covered area is 14% and with a further constraint considering only ablation zone area (Methods Section 1.14, Extended Data Fig. 4, Supplemental Information), debris cover *stage* is 36%. *Stage* ranges from 0 to 1, where a *stage* of 1 means the entire ablation zone of a glacier is covered in debris. This corresponds to reaching the full, 2-D 'debris cover carrying capacity' of a glacier because debris-covered area cannot expand further without up-glacier migration of the equilibrium line.

Alaska, South Asia West and Greenland have the greatest absolute debris-covered area among Earth's glacierized regions and constitute over half of Earth's total supraglacial debris coverage (Fig. 1, Extended Data Table 1). However, when considering regional percentages of debris-covered area, the debris structures within these three top regions reflect markedly different states, where Greenland has a sparse debris cover spread over a wide glacierized area and South Asia

West has a more advanced debris cover distributed over relatively sparse glacierization (Extended Data Table 1). Alaska has a similar percentage of debris cover as South Asia West but with more glacier and debris-covered area by a factor of three (Extended Data Table 1, 2).

We find that an exponential relation describes an increased regional percentage of debris-covered glacier area with decreasing distance from the equator (Fig. 2). This relation suggests that warmer climatic zones are more dynamic and conducive to supraglacial debris production, yet orographic factors (e.g. mountain range age, relief and lithology) may be able to offset a region from this relation as shown by outlying regions in Fig. 2, specifically Alaska.

Debris cover state

To further decompose regional variability, debris coverage and evolutionary state was derived for each individual glacier where certain surface area and debris cover criteria were met (Methods Section 1.13). Two metrics common in glaciological literature were calculated: *percent debris-covered*, and the *accumulation zone area ratio* (*AAR*)[24]. Four new metrics were also calculated that, together, summarize debris cover state: *stage* (described above), *debris expansion potential, future debris expansion* and *moraine abundance* (Fig. 3).

Debris expansion potential is the length of the debris cover-bare ice boundary divided by the perimeter of the debris cover. Drawing on an assumption that newly debris-covered area will share a boundary with existing debris cover (Supplemental Information), the debris cover-bare ice boundary is the location with the highest potential to expand 'inward', flipping formerly bare ice area to debris-covered. The length of this boundary, and thus the glacier normalized *debris expansion potential* value, will increase during a phase of moraine formation where there are potentially several discrete and parallel medial moraines. In a warming climate favorable to an expanding debris cover, *debris expansion potential* will, at some point in time, reach a glacier specific maximum value (≤ 1) at the glacier's peak abundance of discrete moraine bands. Finally, *debris expansion potential* will decrease as once discrete medial moraines coalesces to form a continuous debris cover and reach the spatial debris cover carrying capacity (*stage* = 1). At this point, *debris expansion potential* will have converged to the length of a future equilibrium line divided by the future ablation zone perimeter. The value of *debris expansion potential* at this future convergence is termed the *future expansion potential* which we coarsely estimate for each glacier assuming a static equilibrium line and glacier geometry through time.

Moraine abundance is the ratio of a glacier's debris cover perimeter and the perimeter of its ablation zone. *Moraine abundance* has no structural upper limit and will increase with the abundance and length of distinct medial moraines. This metric is identical to *stage* except that it is expressed in terms of shape perimeters rather than areas and is thus proportional to moraine structure complexity. While *debris expansion potential* is a ratio of two debris related terms, *moraine abundance* is normalized to a debris independent term, the ablation zone area, making it a summary metric that includes aspects of both *stage* and *debris expansion potential*. The time evolution of *moraine abundance* will follow a similar trajectory to *debris expansion potential*, but with convergence to a value of 1 as debris fills the entire ablation zone (reaching the spatial carrying capacity, *stage* = 1) and the two perimeters become identical in shape and length.

While *percent debris-covered* is the universally used metric to describe debris cover, it does not converge to a known shape or quantity and it is less sensitive to debris cover changes due to the inclusion of the accumulation zone in normalization. A selection of four glaciers from around the world with similar surface areas were selected to show both an example of mapped quantities with their corresponding metric values as well as snapshot examples, present on Earth today, of the debris cover evolution progression described above (Fig. 3). The progression of moraine structures, from spare moraines to a near-complete debris cover, is reflected in both *debris expansion potential* and *moraine abundance* and the progression in overall debris cover is captured by *stage*. *Percent debris-covered* fails to capture an evolution progression and reaches an inconspicuous value of 40% even though nearly every part of the glacier that could be debris-covered, is debris-covered. This suggests that, provided an accurate estimate of the equilibrium line can be made (Extended Data Fig. 5, Supplemental Information), the set of metrics derived here should complement or replace results presented as *percent debris-covered*.

Combined, these new metrics transform 2-D structural complexities into a set of 0-D values that can easily integrate into a global scale model. These metrics, computed per glacier, are summarized at a global scale by regional median and percentile statistics (Fig. 4). An isolation of 'advanced' *stage* glaciers, delimited arbitrarily by a *stage* of 0.7, shows their concentrated abundance in Alaska, High Mountain Asia and New Zealand (Fig. 4a). However, for most regions, advanced *stage* glaciers fall outside of the 90% percentile and are thus currently rare within the glacier domain established in the RGI.

Debris cover evolution trajectory

Under the frequently stated assumption that debris-covered area will continue to expand in a warming climate[25,26], *stage* can be considered a proxy for time. A timescale on the order of 100s of years of gradual debris cover expansion[9,27] is likely needed to sum to distinct changes in *stage*, e.g. a transition from sparse debris cover to a glacier's peak abundance of medial moraines. This association with time allows the current global distribution of glaciers exhibiting different values of *stage* to characterize the trajectory of debris cover evolution (Fig. 5,6).

Considering the global distribution of glaciers, continuous space-for-time trajectories of *debris expansion potential* (Fig. 5) and *moraine abundance* (Fig. 6) were derived. For both metrics, the x-axis distance from the maximum value of the trajectory curve to the peak point density, interpreted as a summary value of the bulk regional or global current state, offers an estimate of the debris evolution past maximum (EPM). The remaining x-axis distance to reach a *stage* of 1 is termed the distance to carrying capacity (DCC). On a global scale, most glaciers with debris cover (not weighted by glacier area) have passed a moraine formation maximum (EPM would be zero or negative otherwise) and are over halfway to reaching the spatial debris cover carrying capacity where DCC = 0.4 for both metrics (Fig. 5, 6).

South Asia East, which has the most negative mass balance of the three High Mountain Asia RGI regions[28], also has the most advanced debris cover state on Earth where DCC is 0.3 and 0.2 for *debris expansion potential* and *moraine abundance*, respectively. As a whole, High Mountain Asia hosts the highest abundance of advanced *stage* glaciers (Fig. 4a). While the high relief and climatic setting within High Mountain Asia might be conducive to debris production[29-31], it is unknown if glaciers in other regions on Earth will eventually reach a similarly advanced state in a continued warming climate. Evidence suggests glacier recession couples with an increase in englacial debris exhumed to the surface[25,32] and an increase in debris supplied from unstable slopes exposed from lowering glacier surfaces[29]. For glaciers trending towards cessation on the downward limbs of Fig. 5 and 6, a possible outcome may be the decoupling of remnant, no longer internally deforming, debris-free accumulation zones from heavily debris-covered tongues that could transition to a rock glacier state (Fig. 5, Supplemental Information). Other possible trajectories include rapid glacier shrinkage that outpaces debris cover evolution reducing its overall impact, or a different trajectory that breaks the currently held assumption that the extent of debris cover will expand in a warming climate[25,26]. The remaining 80% of glaciers (by number, with a surface area >2 km^2 and a debris cover <7% and/or <10km^2) where rock debris is not a prominent feature may establish a debris cover in the future, or may be on an alternative trajectory largely free from the effects of debris cover. Resolving this unknown will be of growing significance in a continued warming climate for long-term projections of glacier changes, water resources and sea level rise.

For the 20% of glaciers that have a substantial debris cover, this study establishes the state of debris cover from a global, regional and individual glacier scale in a publicly available database and provides the first estimates of the long-term trajectory of debris cover evolution. We are able to show that a significant portion of the literature focused on "debris-covered glaciers" was biased towards advanced *stage* glaciers (e.g. Langtang, Nogzumpa, Khumbu and Miage glaciers; identified in Fig. 5, 6), which may have limited relevance if used to extend a process understanding to the bulk of debris-covered glacier ice. Of glaciers with a surface area >2 km^2, 4.1% have a *stage* greater than 0.7 encompassing 12.9% of the total 29,182 km^2 of debris-covered area. The remaining 87.1% of debris-covered ice and its evolution through time is where field-based and modeling efforts might be better focused. We now provide a near census dataset the research community can draw from and contextualize the relative importance of debris cover and the spectrum of debris cover configurations found on Earth's glaciers. Results also reveal which limb of the debris evolution curves (Fig. 5, 6) each glacier falls on. This information can aid numerical models of debris cover evolution by indicating if the model framework should nucleate new debris[33] or expand existing debris[34]. At a global scale, the combined factors of surface debris cover and errors within the RGI suggest glacier melt models that neglect these terms may have inaccurate solutions for melt over 10.6% of the global glacier domain. This finding is compounded by the tendency of debris cover to be most abundant and thick at the lower reaches of a glacier where melt rates would, in the absence of debris cover, be the highest[35]. Results from this study enable the removal of a modeled runoff signal from glacier area that does not exist and provides the locations where a more sophisticated treatment of debris modulated glacier melt is needed. A full integration of these terms will facilitate improved projections of water resources from Earth's glaciers[36] and produce a more confident, and likely lower, estimate of glacier-sourced eustatic sea level rise.

Data availability

This studied relied on publicly available data from the NASA/USGS Landsat program: https://earthexplorer.usgs.gov/. The glacier and debris cover data that support the findings of this study are available at https://doi.org/10.5281/zenodo.3866466 and are described in the Supplemental Information.

Code availability

All of the code written for this study is available from the corresponding author upon request.

References

1. Østrem, G. Ice melting under a thin layer of moraine, and the existence of ice cores in moraine ridges. *Geogr. Ann.* **41**, 228-230 (1959).

2. Mattson, L.E. Ablation on debris covered glaciers: an example from the Rakhiot Glacier, Punjab, Himalaya. *Intern. Assoc. Hydrol. Sci.* **218**, 289-296 (1993).

3. Evatt, G.W. et al. Glacial melt under a porous debris layer. *J. Glaciol.* **61**, 825-836 (2015).

4. Hock, R. et al. GlacierMIP–A model intercomparison of global-scale glacier mass-balance models and projections. *J. Glaciol.* **65**, 453-467 (2019).

5. Ragettli, S., Bolch, T. & Pellicciotti, F. Heterogeneous glacier thinning patterns over the last 40 years in Langtang Himal, Nepal. *Cryosphere* **10**, 2075–2097 (2016).

6. Thompson, S., Benn, D. I., Mertes, J. & Luckman, A. Stagnation and mass loss on a Himalayan debris-covered glacier: processes, patterns and rates. *J. Glaciol.* **62**, 467-485 (2016).

7. Benn, D.I., Bolch, T., Hands, K., Gulley, J., Luckman, A., Nicholson, L.I., Quincey, D., Thompson, S., Toumi, R. and Wiseman, S., 2012. Response of debris-covered glaciers in the Mount Everest region to recent warming, and implications for outburst flood hazards. *Earth-Sci. Rev.* **114**, 156-174 (2012).

8. Kirkbride, M.P. Debris-covered glaciers. In: Singh V.P., Singh P., Haritashya U.K. (eds) *Encyclopedia of snow, ice and glaciers. Encyclopedia of Earth Sciences Series*. Springer, Dordrecht (2011).

9. Deline, P. Change in surface debris cover on Mont Blanc massif glaciers after the ‘Little Ice Age’ termination. *Holocene* **15**, 302-309 (2005).

10. Tielidze, L. G. et al. Supra-glacial debris cover changes in the Greater Caucasus from 1986 to 2014. *Cryosphere* **14**, 585-598 (2020).

11. Kellerer□pirklbauer, A., Lieb, G.K., Avian, M. & Gspurning, J. The response of partially debris□covered valley glaciers to climate change: the example of the Pasterze Glacier (Austria) in the period 1964 to 2006. *Geogr. Ann.* **90**, 269-285 (2008).

12. Shukla, A., Gupta, R.P. & Arora, M.K. Estimation of debris cover and its temporal variation using optical satellite sensor data: a case study in Chenab basin, Himalaya. *J. Glaciol.* **55**, 444-452 (2009).

13. Quincey, D.J. & Glasser, N.F. Morphological and ice-dynamical changes on the Tasman Glacier, New Zealand, 1990–2007. *Glob. Planet. Change* **68** 185-197 (2009).

14. Lambrecht, A. et al. A comparison of glacier melt on debris-covered glaciers in the northern and southern Caucasus. *Cryosphere* **5**, 525-538 (2011).

15. Bhambri, R., Bolch, T., Chaujar, R.K. & Kulshreshtha, S.C. Glacier changes in the Garhwal Himalaya, India, from 1968 to 2006 based on remote sensing. *J. Glaciol.* **57**, 543-556 (2011).

16. Glasser, N.F. et al. Recent spatial and temporal variations in debris cover on Patagonian glaciers. *Geomorphology* **273**, 202-216 (2016).

17. Sasaki, O., Noguchi, O., Zhang, Y., Hirabayashi, Y. & Kanae. S. A global high-resolution map of debris on glaciers derived from multi-temporal ASTER images, *Cryosphere Discuss.* Rejected (2016).

18. Scherler, D.,Wulf, H. & Gorelick, N. Global assessment of supraglacial debris□cover extents. *Geophys. Res. Lett.* **45**, 11798-11805 (2018).

19. Rundquist, D. C. et al. The use of Landsat digital information for assessing glacier inventory parameters. *IAHS* **126**, 321-331 (1980).

20. Herreid, S. et al. Satellite observations show no net change in the percentage of supraglacial debris-covered area in northern Pakistan from 1977 to 2014. *J. Glaciol*. **61**, 524-536 (2015).

21. Pfeffer, W. T. et al. The Randolph Glacier Inventory: a globally complete inventory of glaciers. *J. Glacial.* **60**, 537-552 (2014).

22. RGI Consortium *Randolph Glacier Inventory-A dataset of Global Glacier Outlines*: Version 6.0 (Global Land Ice Measurements from Space (GLIMS), 2017).

23. Kraaijenbrink, P. D. A., Bierkens, M.F.P., Lutz, A.F. & Immerzeel, W.W. Impact of a global temperature rise of 1.5 degrees Celsius on Asia's glaciers. *Nature* **549**, 257-260 (2017).

24. Meier, M. F. Proposed definitions for glacier mass budget terms. *J. Glaciol.* **4**, 252-263 (1962).

25. Kirkbride, M. P. & Deline, P. The formation of supraglacial debris covers by primary dispersal from transverse englacial debris bands. *Earth Surf. Process. Landf.* **38**, 1779-1792 (2013).

26. Thakuri, S. et al. Tracing glacier changes since the 1960s on the south slope of Mt. Everest (central Southern Himalaya) using optical satellite imagery. *Cryosphere* **8**, 1297-1315 (2014).

27. Mölg, N., Bolch, T., Walter, A., & Vieli, A. Unravelling the evolution of Zmuttgletscher and its debris cover since the end of the Little Ice Age. *Cryosphere* **13**, 1889-1909 (2019).

28. Brun, F., Berthier, E., Wagnon, P., Kääb, A. & Treichler, D. A spatially resolved estimate of High Mountain Asia glacier mass balances from 2000 to 2016. *Nat. Geosci.* **10**, 668-673 (2017).

29. D. Scherler, B. Bookhagen, M. R. Strecker, Hillslope□glacier coupling: The interplay of topography and glacial dynamics in High Asia. *J. Geophys. Res. Earth Surf.* **116**, F02019 (2011).

30. H. Nagai, K. Fujita, T. Nuimura, A. Sakai, Southwest-facing slopes control the formation of debris-covered glaciers in the Bhutan Himalaya. *Cryosphere* 7,1303-1314 (2013).

31. Banerjee, A. & Wani, B. A. Exponentially decreasing erosion rates protect the high-elevation crests of the Himalaya. *EPSL* **497**, 22-28 (2018).

32. Anderson, R. S. A model of ablation-dominated medial moraines and the generation of debris-mantled glacier snouts. *J. Glaciol.* **46**, 459-469 (2000).

33. Anderson, L. S. & Anderson, R. S. Modeling debris-covered glaciers: response to steady debris deposition. *Cryosphere* **10**, 1105-1124 (2016).

34. Jouvet, G., Huss, M., Funk, M., & Blatter, H. Modelling the retreat of Grosser Aletschgletscher, Switzerland, in a changing climate. *J. Glaciol.* **57**, 1033-1045 (2011).

35. Hambrey, M. J. et al. Sedimentological, geomorphological and dynamic context of debris-mantled glaciers, Mount Everest (Sagarmatha) region, Nepal. *Quat. Sci. Rev.* ***27***, 2361-2389 (2008).

36. Immerzeel, W. W., Lutz, A. F., Andrade, M., Bahl, A., Biemans, H., Bolch, T., Hyde, S., Brumby, S., Davies, B.J., Elmore, A.C. & Emmer, A. Importance and vulnerability of the world's water towers. *Nature* **577**, 364–369 (2020).

Corresponding author

Correspondence and requests for materials should be addressed to Sam Herreid (samherreid@gmail.com).

Acknowledgments

This study was funded by Northumbria University, privately by the first author, and by the European Research Council (ERC) under the European Union's Horizon 2020 research and innovation programme grant agreement No 772751, RAVEN, Rapid mass losses of debris covered glaciers in High Mountain Asia. S.H. thanks Duncan Quincey, Martin Truffer, Jed Brown and Evan Miles for helpful comments and discussions.

Author contributions

S.H. designed and conducted the study, interpreted the results and wrote the manuscript. F.P. secured the institutional funding, helped interpret the results and contributed to writing the manuscript.

Competing interests

The authors declare no competing interests.

Supplementary information

Supplementary Text

Figures S1-S6

Tables S1-S4

Description of Data S1 to S3

Supplementary References

Fig. 1. Global distribution of supraglacial debris cover. The fraction of glacier area covered by rock debris is shown for each glacierized region on Earth along with false positive (FP) and false negative (FN) errors that were identified and corrected within the RGI v6.0. The glacier area considered in this study is shown as both the fraction of the RGI with errors and glaciers smaller than 1 km^2 removed (SamRGI) and the unaltered RGI v6.0. The fraction ‘Earth's glaciers’ indicates the relative size of each region. (**a**) Cumulative distribution function of per glacier debris cover for Earth's glaciers with a surface area > 2 km^2 suggesting debris cover is present (>0.1 km^2) on 44% of Earth's glaciers and prominent (>1.0 km^2) on 15% of glaciers. (**b**) The Greenland ice sheet is approximately a factor of 4.2 times the surface area of all mountain glaciers combined.

Fig. 2. Polar regions have less debris cover. Exponential function, of the form $y=ae^{-bx}$, fit to regional percent debris-covered glacier area and the absolute value of median latitude (grey bars show full latitude range). Weighted by glacierized area (circle size shows glacierized area scaled linearly). The blue curve is fit using all regions excluding Greenland, the black curve is fit using all regions excluding Greenland and Alaska.

Fig. 3. Source data composite images and examples from different locations on Earth with different metric values. Glaciers were selected based on similar surface area (Ayunnamat Glacier an exception, 20 km^2 less than the other three), and exhibiting the spectrum of metric values ordered (left to right) to show a conceptual progression of debris cover evolution. Notably, the evolution of *moraine abundance* with respect to *stage* (values in grey and purple, respectively) while the often reported metric *percent debris-covered* remains largely stable. Latitude and longitude locate each glacier's centroid. Metric definitions and their constituent glacier quantities are identified on Kangjiaruo Glacier (28.428°N, 85.692°E, South Asia East) which are color coded to each glacier's set of metric values. Equilibrium line is shown on the Landsat composite images to illustrate the quality of this estimate.

Fig. 4. Regional distributions of six metrics relating to glacier health and debris cover configuration. Definitions of the six metrics derived from glacier quantities identified on Kangjiaruo Glacier and neighboring Langtang Glacier (28.305°N, 85.702°E) are color coded to the distributions of each metric for each RGI region. For each distribution, the black dot is the median, the wide colored box outlined in black is 33-66% of the data and the thin colored bar constrains the 10-90th percentile. Numbers in parenthesis are the number of glaciers within each metric's distribution limited by each metric's derivation criteria (Methods Section 1.13). *Debris expansion potential* measured from the present time (blue) will approach the distribution of *future debris expansion* (black, plotted on the same line showing only the median and 10-90th percentile) if debris cover can be assumed to continue to expand in a warming climate. (**a**) The regional distribution and local abundance of the number of glaciers with an 'advanced' (>0.7) *stage*. Langtang Glacier falls within this constraint.

Fig. 5. Using current *stage* and *debris expansion potential* to anticipate the trajectory of debris cover evolution. *Debris expansion potential* passes through the origin, reaches a maximum value (around 0.6) and converges to the true value of *future debris expansion* as *stage* approaches 1. Our estimate of *future debris expansion* is plotted as an orange dot (median) and bar (10-90th percentile). Black points and bars show a moving median and the 10-90th percentiles, respectively. Regions with fewer glaciers had a wider moving median and moving windows with <10 glaciers were skipped. The orange line is a spline fit to the moving median values and forced through the metric constraints. Where $n > 500$ the points are colored to show relative density. Percentages below each plot give the regional fraction of glaciers that meet the criteria for metric derivation. The grey bar gives the range of the absolute value of latitude, or distance from equator. Some seminal glaciers in debris cover research are shown along with the four glaciers in Fig. 3.

Fig. 6. Using current *stage* and *moraine abundance* to anticipate the trajectory of debris cover evolution. *Moraine abundance* follows a similar trajectory to *debris expansion potential* but has no structural upper limit and converges to 1 as *stage* approaches 1. Regions with a lower abundance of glaciers are shown in the Supplemental Information. Plot configuration is the same as described in Fig. 5.

1 Methods

1.1 Satellite image selection

Landsat images were manually selected based on five criteria where relative significance is ranked from 1 to 5:

1. Clouds (minimum coverage over glacierized areas)
2. Seasonal snow cover (minimum)
3. Time (most recent)
4. Sensor (newest, highest NASA assigned quality metric)
5. Abundance of glacierized area within an image (maximum)

The result of this selection process produced a 255 image library of Landsat satellite imagery optimized for debris cover mapping at the most recent date possible (image library assembled in 2016) (Extended Data Fig. 1, Supplemental Information, Data S2). No images were used from Landsat 7 after the Scan Line Corrector failure on 31 May 2003.

<u>1.2 Glacier area cloud mask</u>

While satellite images were selected on a minimum cloud cover criterion, some cloud cover tolerance was necessary for images where no scene in the Landsat archive was entirely cloud free. In order to include the portion of a scene that is cloud free while discarding the clouded areas, a cloud mask was generated manually over glacierized areas for every satellite image.

<u>1.3 Landsat composite without overlap</u>

Within the set of Landsat satellite images selected for this study, there is considerable overlap between neighboring images, especially towards the poles (Extended Data Fig. 1). If debris were mapped for each image and merged into one regional or global debris map, the temporal discontinuity between overlapping portions could cause one of two errors: (1) double counting debris that has been translated perpendicular to glacier flow; or (2) incorrectly associate a map date to a debris cover whose geometry has evolved. To avoid double counting and to assign the correct map date to every debris shape, areas of overlap were removed in a 3-step automated process:

1. **Remove sawtooth edges of Landsat 5 and Landsat 7 data.** Some edges of Landsat 5 and 7 images have a zone with a mix of data, no data and pixels with arbitrary values.

This zone would produce a complex seam if merged with a neighboring image. These edge zones were automatically removed where present by computing an outward buffer of the scene footprint perimeter by a distance equal to the width of the sawtooth zone, buffering the result back by the same distance and clipping the image to this updated shape.

2. **Preference to most recent image.** Where satellite image overlap exists, the more recent image is given preference and the earlier date image is trimmed to share, but not cross, a border with the later image. Before an image is trimmed, all possible neighbor images are tested to optimize coverage with the most recent image. This was achieved by assigning the image acquisition date to each image footprint in shapefile format and then iterating through every image, locating neighbor images that have a nonzero intersection and removing the overlap area from the image with the earliest acquisition date.

3. **Cloud mask holes filled.** Where the most recent scene is given preference from Step 2 but contains a no-data hole removed from the cloud mask (see above), the code attempts to fill the hole with the next most recent underlying image if overlap exists at this location. This was automated by iterating though neighbor images looking for older, overlapping images that intersect the image specific cloud mask.

The result of this fully automated process is an overlap-free Landsat composite dataset with preference to the most recently acquired satellite image and a clear data acquisition date assigned to every location and subsequently every debris map shape generated from these data. Extended Data Fig. 2 shows an example output of this process for Alaska.

1.4 1 km^2 minimum glacier area restriction for debris cover mapping

The minimum glacier area considered for debris mapping was 1 km^2. A substantial amount of manual effort was conducted on an individual glacier basis for all regions on Earth. The motivation for this area limit is that a consideration of glaciers smaller than 1 km^2 would have been both time consuming and difficult to hold to a quality level consistent with bigger glaciers. Glaciers with a surface area less than 1 km^2 sum to 39,583.2 km^2 or 8.2% of the RGI v6.0 excluding Greenland and Antarctica.

1.5 Translation error in RGI v6.0

Within the RGI v6.0 dataset, some translation errors were detected where glacier outlines appeared to have a linear or nonlinear shift relative to Landsat imagery when projected in the same (image specific UTM zone) coordinate system. Linear offsets were manually corrected and nonlinear offsets were crudely corrected by shifting individual or clusters of glaciers, where a glacier was the smallest element that was manipulated. No further alterations were made during this step except the removal of glacier overlap to avoid topological errors and double counting of glacier area. The two regions where translation errors were most present were 03 Arctic Canada North and 04 Arctic Canada South where a high latitude amplification of geolocation errors from variable projections used during mapping efforts is a probable cause. Considering the sum of false positive (FP) and false negative (FN) errors introduced by shifted glacier outlines, the error for these two regions are 4434.3 km^2 (4.4% of the region) and 71.3 km2 (0.2%), respectively.

Because translation error is not directly related to specific glacier shapes, these values were not included in the total RGI errors presented in Table S2.

1.6 Initial debris cover map

With each satellite image trimmed to a geometry that fits seamlessly with its neighbors (Extended Data Fig. 1, 2), an initial, first iteration debris map was generated. Debris cover was mapped following a well-established method[18-20] where: 1. off glacier area was removed from the raw near-infrared (NIR) and Short-wave infrared (SWIR) bands for each satellite image; 2. the band ratio NIR/SWIR was computed; and 3. a pixel-based threshold value discriminating between debris-covered and debris-free glacier area was applied. While the optimum threshold value for mapping debris cover will vary between satellite images[20], only one threshold value, 1.57 (a value found optimal for a Landsat 8 image in Northern Pakistan by (ref. [3])), was used across all scenes and all three Landsat sensors used. Results using a single threshold value was deemed satisfactory for the scope and scale of this project (Supplemental Information) and is consistent with other large-scale debris mapping studies[18,37,38]. This initial, global-scale debris map provided the basis for the identification and removal of false positive (FP) errors both in the debris map as well as in the RGI v6.0.

1.7 FP errors in the initial debris cover map and the RGI

While the output of the initial debris cover map identified debris-covered portions of Earth's glaciers, it also classifies bedrock nunataks, non-glacierized land and heavily shaded areas (lightly shaded regions should be mitigated by the band ratio) as debris cover. Depending on the quality of the glacier outlines and the sun angle during the time of satellite image acquisition coupled with the amplitude of the surrounding topography, these errors can be substantial. To both quantify and remove these errors a series of manual identification steps were conducted.

The geometry of a nunatak or non-glacierized feature located within a glacier shape is accurately defined in the initial debris map. By on-screen, visual inspection against the Landsat composite imagery, a decision was made whether each shape in the initial debris map was true positive (TP) or FP debris cover. This decision was logged by drawing a wider shape, or lasso, around all FP area. This was done for all glaciers on Earth in a manually intensive effort by one person (S. Herreid) for consistency. For the second iteration debris map, area that fell within a FP lasso was not considered part of the glacier domain while area outside of the FP lasso was again mapped as TP debris-covered glacier area (Extended Data Fig. 3).

1.8 False negative errors added to the RGI v6.0

Since the RGI v6.0 is a composite dataset of automated routines, semi-automated routines and manual glacier digitization by many individuals[21] with a variable definition of what a glacier is and variable expertise (both human and algorithm) in including debris-covered termini, there are instances where substantial portions of a glacier are excluded from the inventory. Additionally, real glacier area changes can be substantial over very short time intervals and frontal positions can evolve on the order of kilometers between the source data used to produce the RGI and the Landsat composite used in this study.

While many ambiguities cloud the definition of a glacier and the boundary defining a debris-covered terminus, wider glaciological conclusions built upon sharp boundaries drawn within these ambiguities are aided by consistency. Subjectivity in manual differentiation is unavoidable, particularly for debris-covered areas[39], but by having only one person manually assess and alter the entire RGI, the final refined result is likely to be a more consistent product.

To incorporate RGI false negative (FN) glacier area present in the Landsat satellite composite dataset, missing areas were manually digitized (red outlined shapes in Extended Data Fig. 3). FN area added was not exclusively debris-covered and thus required a second debris cover classification iteration using the updated glacier area as input.

1.9 Shaded area causing FP debris to be mapped in TP bare ice area

Areas mapped as debris in the initial debris map that were in reality optically dark, bare glacier ice due to shading were manually identified similar to the treatment of FP errors. The shaded error, however, were only removed from the debris cover results and the intersecting RGI area was left intact. For locations where a cast shadow confused the automated debris mapping algorithm but a distinction could be made visually, the identifying shape was manually drawn to preserve the debris structure, thus removing only the bare ice portion of the shaded area from the debris map. The area of FP debris mapped in TP bare ice area is ephemeral and not intrinsic to any derived dataset, yet we include the total shadow area removed in Extended Data Table 2 to document the magnitude of this factor.

1.10 Exclusion of Antarctica and unique considerations for Greenland

Antarctica, where debris cover is anticipated to be sparse, was excluded from this study, while debris cover observed in Greenland prompted the inclusion of the entire Greenland ice sheet, beyond the RGI's inclusion of only periphery glaciers. RGI v6.0 Greenland Periphery glacier outlines were given preference to, and merged with Greenland ice sheet outlines from[40]. Due to incongruities of this merged product and the exceptionally large size of this region, a simplified approach to removing glacier outline error was used for Greenland to speed up the derivation of a debris cover map. Rather than identifying errors (e.g. method shown in Extended Data Fig. 3), TP debris area was identified manually. Debris shapes outside of those manually identified as TP were not removed or differentiated between FP area, area in shadow, clouded area and networks of surface ponds. This approach allowed the quality of the debris maps to be equal to those of the other RGI regions on Earth but disabled the ability to quantify ice outline errors.

1.11 Final debris map with a refined version of the RGI

With all of the FP error area removed and FN error area added, an updated and refined version of the RGI (termed 'SamRGI' for clarity) was produced and used as input for a final iteration of the debris mapping algorithm. While the debris maps were generated for each (trimmed) Landsat scene separately in the image specific UTM zone, the final regional debris maps were merged and projected into a set of continental scale map projections selected to offer accurate area calculations (Supplemental Information).

1.12 Fraction of RGI v6.0 and SamRGI considered

The fraction of RGI v6.0 considered is defined as the ratio of the following two quantities:

- Unaltered RGI v6.0 regional area with glaciers <1 km^2 removed and area that does not intersect the Landsat image composite removed.

- unaltered RGI v6.0 regional area.

This provides an estimate of the fraction of all glaciers, including those with a surface area <1 km^2, that are considered in this study. The value is not penalized for FP area that is later removed to improve the RGI.

The fraction of SamRGI considered does not penalize for glacier <1 km^2 being removed and incudes all of the glacier geometry edits made in this study. It is defined as the ratio of:

- Altered RGI v6.0 regional area with glaciers <1 km^2 removed and area that does not intersect the Landsat image composite removed.

- Altered RGI v6.0 regional area with glaciers <1 km^2 removed both inside and outside of the Landsat image composite.

1.13 Criteria for computing the debris cover metrics

The criteria for metric computation varied per metric and was most restrictive for metrics that depend on estimates of the equilibrium line.

- **2 km^2 minimum glacier area** For the computation of all metrics (*AAR*, *stage*, *debris expansion potential*, *future expansion potential*, *percent debris-covered* and *moraine abundance*), glaciers with a surface area less than 2 km^2 were excluded. This was done to statistically increase the TP rate of the debris maps. Larger glaciers have a larger capacity for debris coverage and more debris pixels increases the probability of a high TP debris classification rate.

- **Minimum 7% debris-covered unless debris-covered area is greater than 10 km^2** For glaciers where *percent debris-covered* was less than 7%, computations of *AAR*, *stage*, *future expansion potential* and *moraine abundance* were discarded (metric values set to -9999). This limit was selected in an attempt to only consider glaciers where there was a higher probability that the debris extent extended close to the true equilibrium line (Supplemental Information) while also being as low of a value as possible to maximize inclusivity. This limit was discarded in cases where a glacier's summed debris-covered area was 10 km^2 or greater to include large glaciers with a likely developed and confidently mapped debris cover, but a debris-covered percentage falling below the 7% threshold.

- **A non-existent debris cover cannot "expand"** Where *debris expansion potential* was measured to be 0 (in a case of no mapped debris cover) the metric value was set to -9999 indicating that the potential of a debris cover to expand is unknown/not applicable.
- ***Future expansion potential* cannot be negative** *Future expansion potential* was set to -9999 where it was computed as a negative value.

1.14 Equilibrium line estimate from debris exposure

Debris cover that is exposed at the surface of a glacier for longer than one year is, by definition, located within the ablation zone. Debris that is exposed at the surface of a glacier for less than one year while remaining an element of the glacier for more than one year is, by definition, located within the accumulation zone. Drawing on these two axioms and one fundamental assumption, debris cover can be used to define an equilibrium line estimate. The assumption is that a glacier with a sufficient debris-covered area (defined here as glaciers with 7% debris cover and/or >10 km^2 of debris-covered area) will have (at least some) debris inputs above the equilibrium line and some of that debris will be exhumed to the surface at, or near (below), the equilibrium line. If the top, up-glacier extent of a debris cover can be expanded orthogonal to glacier flow to the full glacier width and shifted up-glacier to correct for the englacial flow path of debris that is not deposited onto the glacier exactly at the equilibrium line, an equilibrium line estimate can be defined (Extended Data Fig. 4).

To transform mapped debris geometry (which can be any shape, e.g. medial moraine bands, lateral moraines or complete coverage of the glacier width) to a top of the debris coverage line that spans the full glacier with, a buffer function was applied. In the cases of several medial moraine bands or complete debris coverage, the process is more simplistic: an outward extension of the debris shapes a short distance will overlap/merge to form a synthetically debris filled ablation zone. In the most difficult case, where there is one narrow lateral moraine on only one side of a glacier, the buffer distance will need to extend the full width of the glacier to achieve the same, desired, synthetically full ablation zone. Following this logic, a buffer-out distance that is appropriate for a small glacier will be insufficient for a large glacier and a buffer-out distance for a large glacier will be excessive for a small glacier. To account for both this size variability and the case of only one lateral moraine, we use the readily known quantity glacier area to roughly estimate glacier width (Supplemental Information) which we set as our buffer-out distance, d_{out}. After generating a synthetically full debris-covered ablation zone with d_{out}, the ablation zone shape is buffered back inward a distance d_{in}. Following the guiding hypothesis that a sufficiently debris-covered glacier will have mappable debris located near the ablation zone (Supplemental Information), we correct for an anticipated swath of bare glacier ice that separates the first mappable debris cover and the true equilibrium line by a distance d (Extended Data Fig. 4). This correction is made by the relation $d_{in} = x d_{out}$ where x is a defined coefficient between 0 and 1 that enables an estimate of d, where $d = (1\text{-}x)$*glacier width*.

Using $x = 0.75$ (Supplemental Information) and estimated glacier widths, an ablation zone was derived for every glacier on Earth with a surface area >2 km^2. Glaciers that did not meet the 7% debris cover and/or >10 km^2 debris-covered area criteria were deemed unlikely to have sufficient debris cover to successfully define an ablation zone and were excluded from further analysis.

References

37. Kienholz, C. et al. Derivation and analysis of a complete modern-date glacier inventory for Alaska and northwest Canada. *J. Glaciol.* **61**, 403-420 (2015).
38. Mölg, N., Bolch, T., Rastner, P., Strozzi, T., & Paul, F. A consistent glacier inventory for Karakoram and Pamir derived from Landsat data: distribution of debris cover and mapping challenges. *ESSD* **10**, 1807-1827 (2018).
39. Paul, F. et al. On the accuracy of glacier outlines derived from remote-sensing data. *Ann. Glaciol.* **54**, 171-182 (2013).
40. Citterio, M. & Ahlstrøm, A. P. The aerophotogrammetric map of Greenland ice masses. *Cryosphere* **7**, 445-449 (2013).

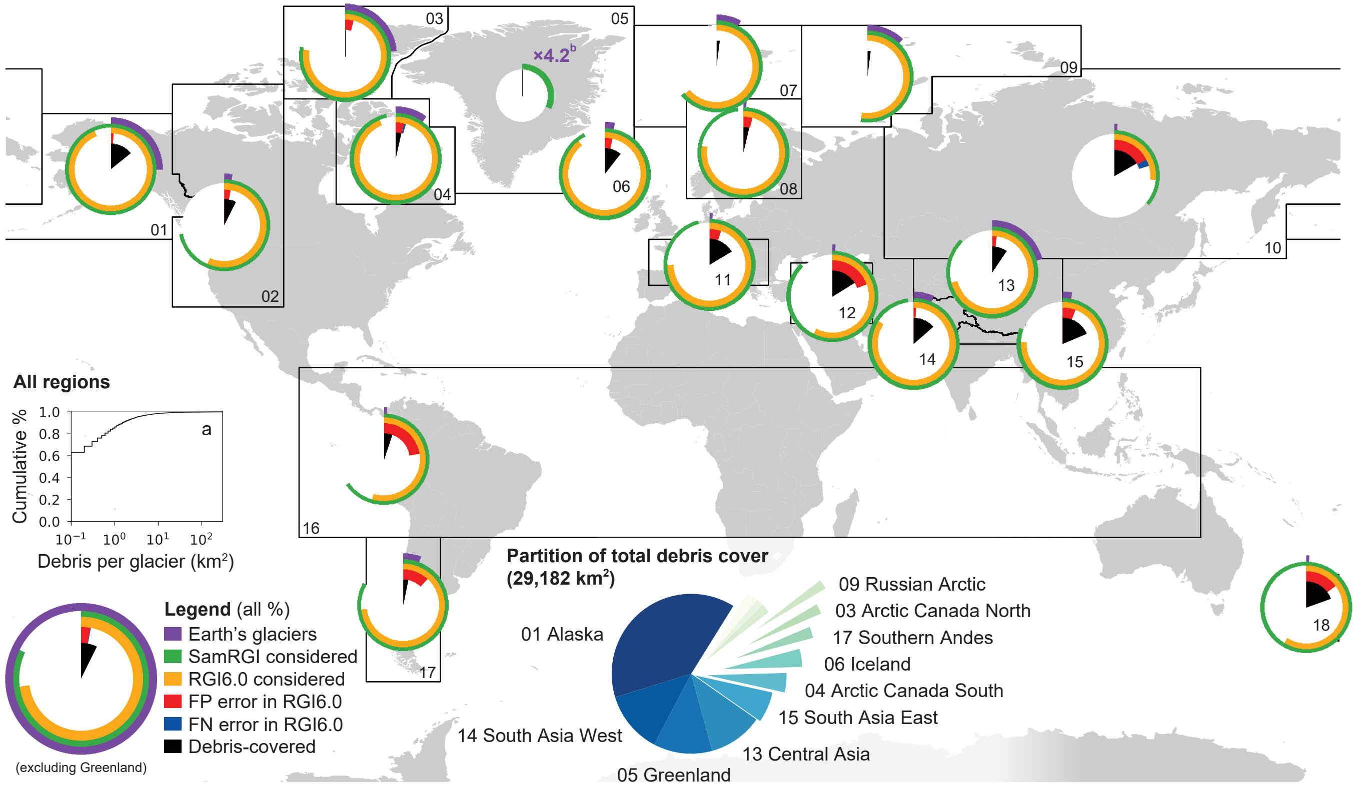

03
05
×4.2[b]
07
09
01
02
04
06
08
10
11
12
13
14
15
16
17
18
All regions
a
Cumulative %
1.0
0.8
0.6
0.4
0.2
0.0
10^{-1} 10^{0} 10^{1} 10^{2}
Debris per glacier (km^2)
Legend (all %)
Earth's glaciers
SamRGI considered
RGI6.0 considered
FP error in RGI6.0
FN error in RGI6.0
Debris-covered
(excluding Greenland)
Partition of total debris cover
(29,182 km^2)
09 Russian Arctic
03 Arctic Canada North
17 Southern Andes
06 Iceland
04 Arctic Canada South
15 South Asia East
13 Central Asia
05 Greenland
14 South Asia West
01 Alaska

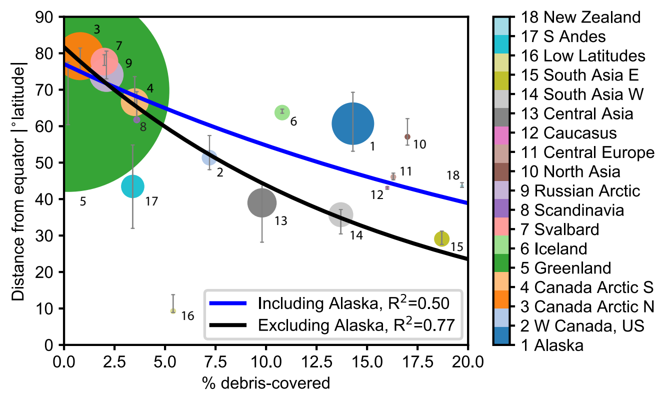

Distance from equator |°latitude|
% debris-covered
0
10
20
30
40
50
60
70
80
90
0.0
2.5
5.0
7.5
10.0
12.5
15.0
17.5
20.0
Including Alaska, R^2=0.50
Excluding Alaska, R^2=0.77
1
2
3
4
5
6
7
8
9
10
11
12
13
14
15
16
17
18
18 New Zealand
17 S Andes
16 Low Latitudes
15 South Asia E
14 South Asia W
13 Central Asia
12 Caucasus
11 Central Europe
10 North Asia
9 Russian Arctic
8 Scandinavia
7 Svalbard
6 Iceland
5 Greenland
4 Canada Arctic S
3 Canada Arctic N
2 W Canada, US
1 Alaska

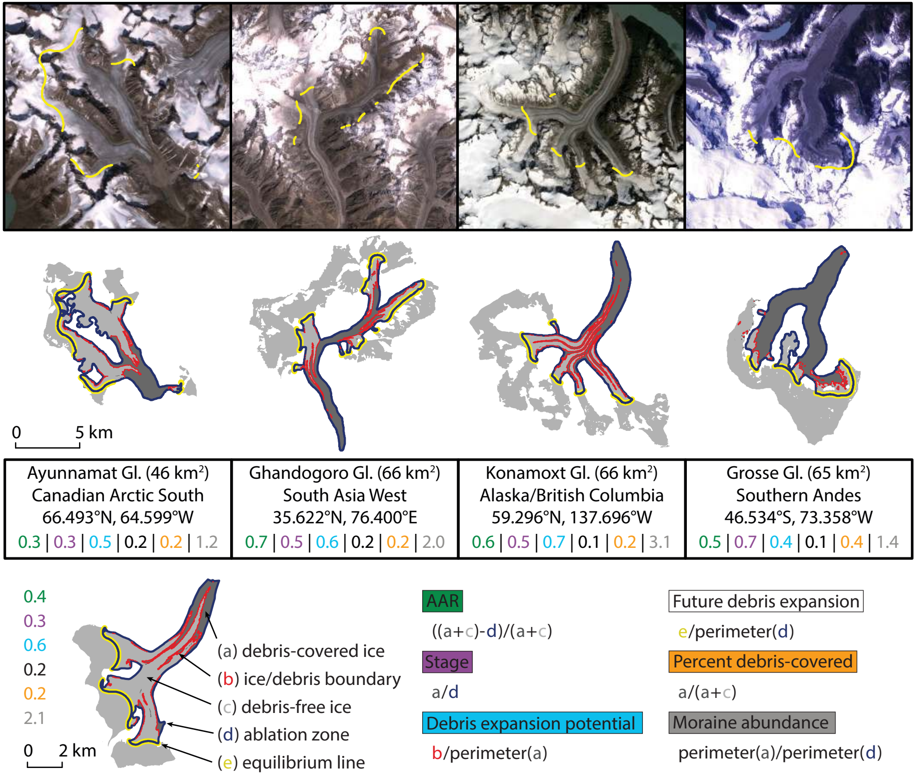
0
5 km
Ayunnamat Gl. (46 km²)
Canadian Arctic South
66.493°N, 64.599°W
0.3 | 0.3 | 0.5 | 0.2 | 0.2 | 1.2
Ghandogoro Gl. (66 km²)
South Asia West
35.622°N, 76.400°E
0.7 | 0.5 | 0.6 | 0.2 | 0.2 | 2.0
Konamoxt Gl. (66 km²)
Alaska/British Columbia
59.296°N, 137.696°W
0.6 | 0.5 | 0.7 | 0.1 | 0.2 | 3.1
Grosse Gl. (65 km²)
Southern Andes
46.534°S, 73.358°W
0.5 | 0.7 | 0.4 | 0.1 | 0.4 | 1.4
0.4
0.3
0.6
0.2
0.2
2.1
0
2 km
(a) debris-covered ice
(b) ice/debris boundary
(c) debris-free ice
(d) ablation zone
(e) equilibrium line
AAR
((a+c)-d)/(a+c)
Stage
a/d
Debris expansion potential
b/perimeter(a)
Future debris expansion
e/perimeter(d)
Percent debris-covered
a/(a+c)
Moraine abundance
perimeter(a)/perimeter(d)

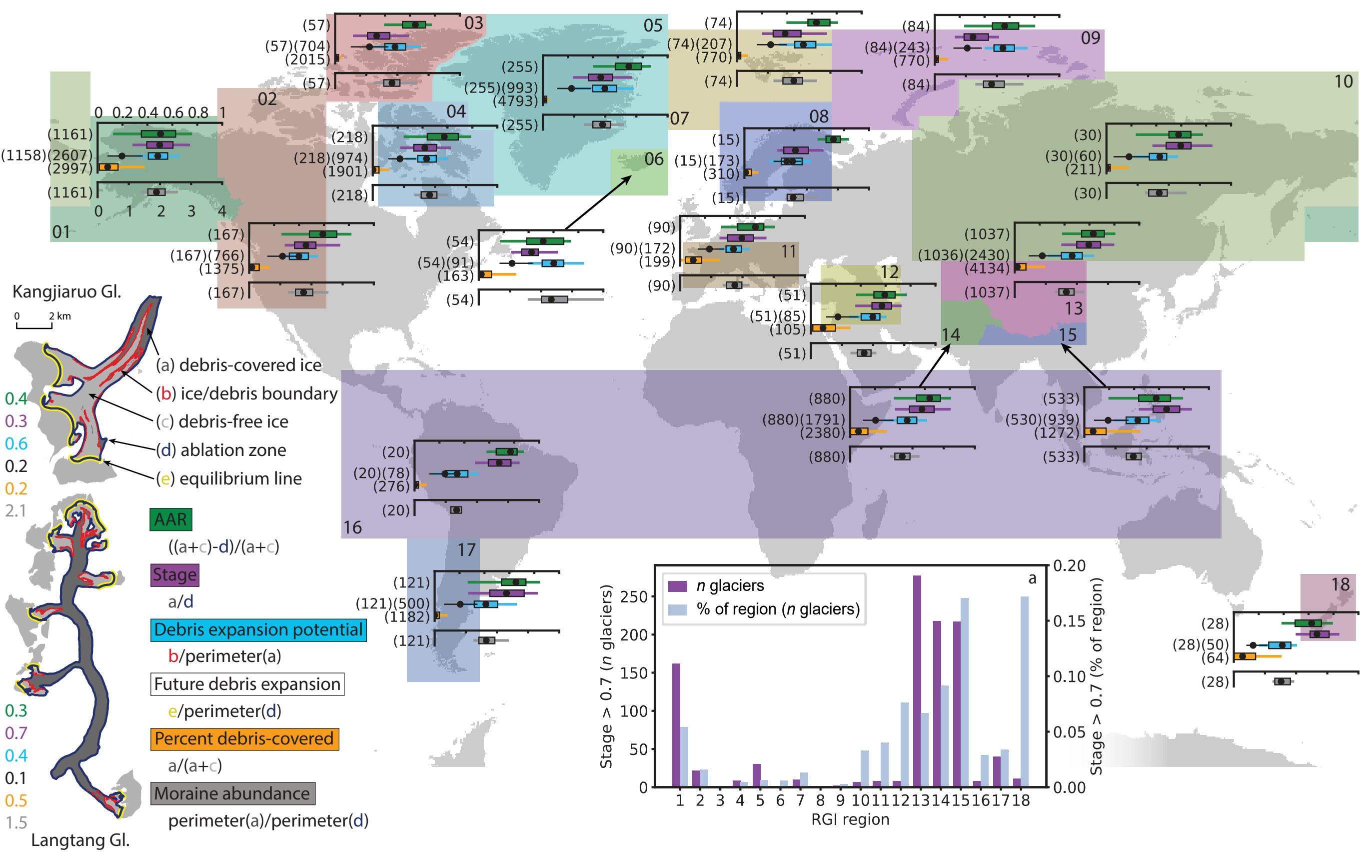

01
02
03
04
05
06
07
08
09
10
11
12
13
14
15
16
17
18
0 0.2 0.4 0.6 0.8 1
0 1 2 3 4
(1161)
(1158)(2607)
(2997)
(1161)
Kangjiaruo Gl.
0 2 km
(a) debris-covered ice
(b) ice/debris boundary
(c) debris-free ice
(d) ablation zone
(e) equilibrium line
0.4
0.3
0.6
0.2
0.2
2.1
0.3
0.7
0.4
0.1
0.5
1.5
Langtang Gl.
AAR
((a+c)-d)/(a+c)
Stage
a/d
Debris expansion potential
b/perimeter(a)
Future debris expansion
e/perimeter(d)
Percent debris-covered
a/(a+c)
Moraine abundance
perimeter(a)/perimeter(d)
n glaciers
% of region (n glaciers)
a
Stage > 0.7 (n glaciers)
Stage > 0.7 (% of region)
RGI region
0 50 100 150 200 250
0.00 0.05 0.10 0.15 0.20
1 2 3 4 5 6 7 8 9 10 11 12 13 14 15 16 17 18

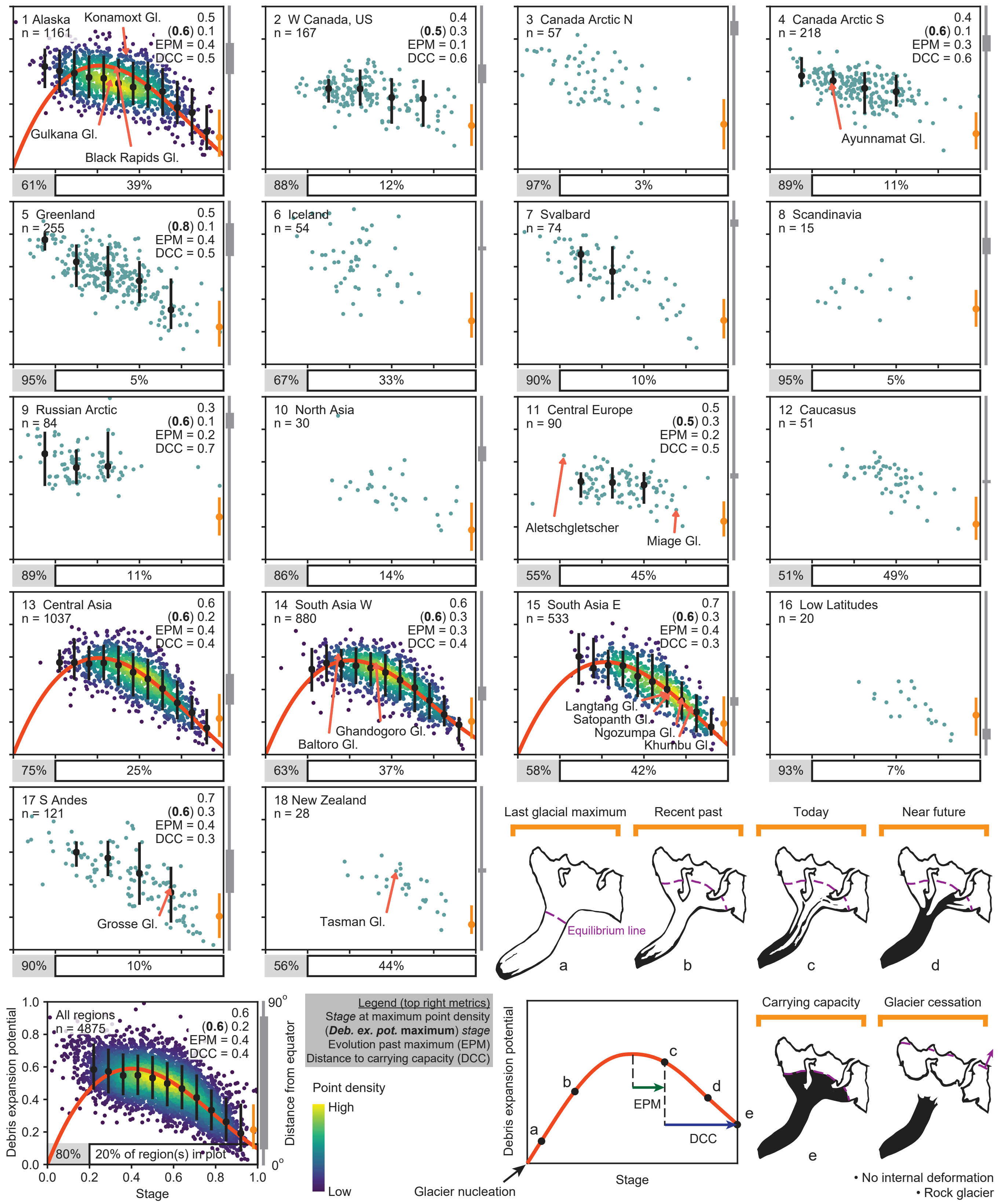

1 Alaska
n = 1161
Konamoxt Gl.
0.5
(0.6) 0.1
EPM = 0.4
DCC = 0.5
Gulkana Gl.
Black Rapids Gl.
61%
39%
2 W Canada, US
n = 167
0.4
(0.5) 0.3
EPM = 0.1
DCC = 0.6
88%
12%
3 Canada Arctic N
n = 57
97%
3%
4 Canada Arctic S
n = 218
0.4
(0.6) 0.1
EPM = 0.3
DCC = 0.6
Ayunnamat Gl.
89%
11%
5 Greenland
n = 255
0.5
(0.8) 0.1
EPM = 0.4
DCC = 0.5
95%
5%
6 Iceland
n = 54
67%
33%
7 Svalbard
n = 74
90%
10%
8 Scandinavia
n = 15
95%
5%
9 Russian Arctic
n = 84
0.3
(0.6) 0.1
EPM = 0.2
DCC = 0.7
89%
11%
10 North Asia
n = 30
86%
14%
11 Central Europe
n = 90
0.5
(0.5) 0.3
EPM = 0.2
DCC = 0.5
Aletschgletscher
Miage Gl.
55%
45%
12 Caucasus
n = 51
51%
49%
13 Central Asia
n = 1037
0.6
(0.6) 0.2
EPM = 0.4
DCC = 0.4
75%
25%
14 South Asia W
n = 880
0.6
(0.6) 0.3
EPM = 0.3
DCC = 0.4
Ghandogoro Gl.
Baltoro Gl.
63%
37%
15 South Asia E
n = 533
0.7
(0.6) 0.3
EPM = 0.4
DCC = 0.3
Langtang Gl.
Satopanth Gl.
Ngozumpa Gl.
Khumbu Gl.
58%
42%
16 Low Latitudes
n = 20
93%
7%
17 S Andes
n = 121
0.7
(0.6) 0.3
EPM = 0.4
DCC = 0.3
Grosse Gl.
90%
10%
18 New Zealand
n = 28
Tasman Gl.
56%
44%
Last glacial maximum
Recent past
Today
Near future
Equilibrium line
a
b
c
d
All regions
n = 4875
0.6
(0.6) 0.2
EPM = 0.4
DCC = 0.4
80%
20% of region(s) in plot
Debris expansion potential
Stage
0.0
0.2
0.4
0.6
0.8
1.0
90°
0°
Distance from equator
Legend (top right metrics)
Stage at maximum point density
(Deb. ex. pot. maximum) stage
Evolution past maximum (EPM)
Distance to carrying capacity (DCC)
Point density
High
Low
Debris expansion potential
Stage
a
b
c
d
e
EPM
DCC
Glacier nucleation
Carrying capacity
Glacier cessation
e
• No internal deformation
• Rock glacier

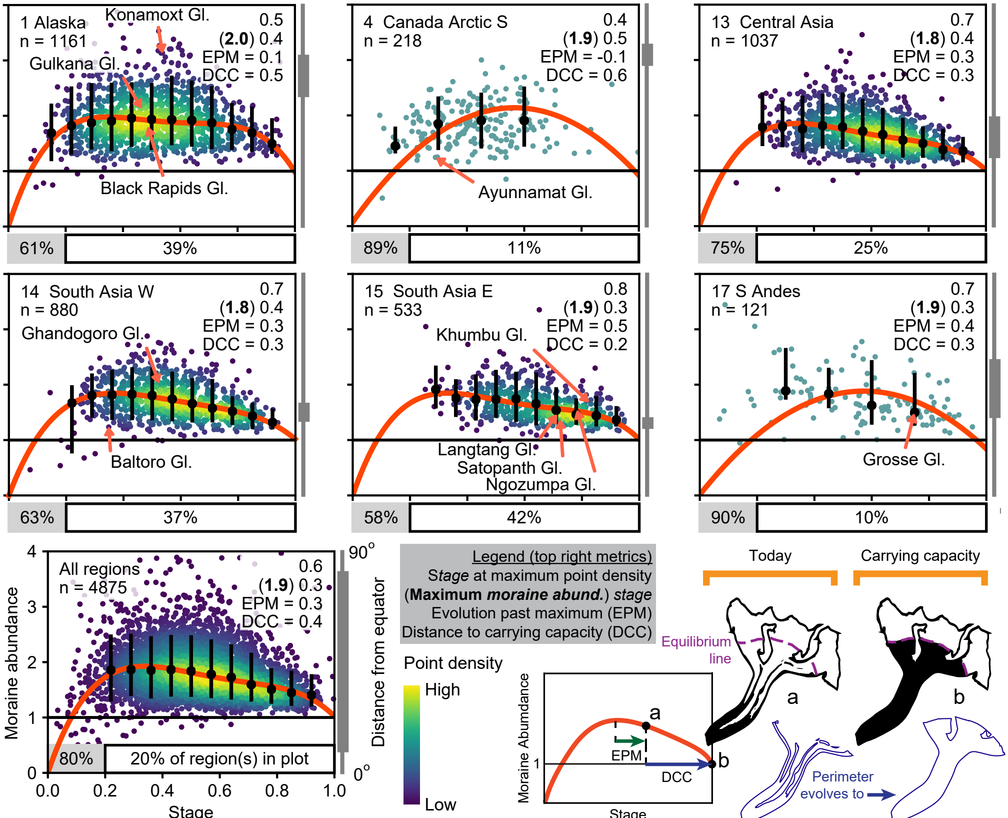

1 Alaska
n = 1161
Konamoxt Gl.
0.5
(**2.0**) 0.4
EPM = 0.1
DCC = 0.5
Gulkana Gl.
Black Rapids Gl.
61%
39%
4 Canada Arctic S
n = 218
0.4
(**1.9**) 0.5
EPM = -0.1
DCC = 0.6
Ayunnamat Gl.
89%
11%
13 Central Asia
n = 1037
0.7
(**1.8**) 0.4
EPM = 0.3
DCC = 0.3
75%
25%
14 South Asia W
n = 880
0.7
(**1.8**) 0.4
EPM = 0.3
DCC = 0.3
Ghandogoro Gl.
Baltoro Gl.
63%
37%
15 South Asia E
n = 533
0.8
(**1.9**) 0.3
EPM = 0.5
DCC = 0.2
Khumbu Gl.
Langtang Gl.
Satopanth Gl.
Ngozumpa Gl.
58%
42%
17 S Andes
n = 121
0.7
(**1.9**) 0.3
EPM = 0.4
DCC = 0.3
Grosse Gl.
90%
10%
All regions
n = 4875
0.6
(**1.9**) 0.3
EPM = 0.3
DCC = 0.4
80%
20% of region(s) in plot
Moraine abundance
Stage
Distance from equator
90°
0°
Legend (top right metrics)
Stage at maximum point density
(**Maximum *moraine abund.***) *stage*
Evolution past maximum (EPM)
Distance to carrying capacity (DCC)
Point density
High
Low
Today
Carrying capacity
Equilibrium line
a
b
Moraine Abundance
EPM
DCC
Stage
Perimeter evolves to